Electrical Power and Energy Systems 125 (2021) 106551

Contents lists available at ScienceDirect

International Journal of Electrical Power and Energy Systems

journal homepage: www.elsevier.com/locate/ijepes

Steady-state security region of energy hub: Modeling, calculation, and applications

Pei Yong [a,d], Yi Wang [b], Tomislav Capuder [c], Zhenfei Tan [a,d], Ning Zhang [a,d,*], Chongqing Kang [a,d]

[a] Department of Electrical Engineering, Tsinghua University, Beijing, 100084, China
[b] Department of Information Technology and Electrical Engineering, ETH Zurich, Zurich, 8092, Switzerland
[c] Department of Energy and Power Systems, Faculty of Electrical Engineering and Computing, University of Zagreb, Unska 3, HR-10000 Zagreb, Croatia
[d] International Joint Laboratory on Low Carbon Clean Energy Innovation

ARTICLE INFO

Keywords:
Multi-energy systems (MES)
Energy hub (EH)
Load carrying capability
Security region
Projection

ABSTRACT

Multi-energy systems (MES) provide various types of energy services by coupling different energy sectors. Such coupling increases the efficiency and flexibility of the entire energy system, and at the same time, however, increases the dependencies of the load carrying capability among different types of load demand. In the MES planning stage, we always want to assess and compare the load carrying capability among different planning schemes, considering the N-1 or N-M contingencies and the mutual effect of different energy sectors. While in the MES operation stage, we always want to know if the load of MES can be securely supplied considering potential contingencies and how far the current operation status is from the security boundary. This paper proposes a new concept named the energy hub (EH) security region and applying the concept to depict the load carrying capability of the district MES. The concept defines a region in a hyperspace where the MES can be safely operated under steady-state operational and security constraints. We first model the district MES using the EH approach and propose the mathematical form of the EH steady-state security region systematically. Then, a vertex-based algorithm is proposed to precisely calculate the security region using a space projection technique. We further propose indices to evaluate the load carrying capability of a district MES and identify critical components. Numerical case studies are conducted on two test systems to verify the validity of the proposed method. The results show the proposed EH security region concept and calculation method provide quantitive indicators on how to compare MES planning schemes and improve the load carrying capability.

1. Introduction

Multi-energy systems (MES) incorporate the production, conversion, transmission, and utilization of multiple energy sources in a unified manner and improve the overall energy efficiency [1,2]. While increasing the flexibility of the energy systems, the coupling of different energy sectors causes dependencies of the load carrying capability of different types of load demand. Take the combined heat and power (CHP) unit as an example, its electricity and heat load carrying capabilities, which measure the maximum electricity and heat load that can be served respectively [3], are coupled, so that the failure of a CHP would influence the load carrying capabilities of both the electricity and heat sectors. Moreover, different kinds of load demands are correlated and the dependencies among them cannot be ignored. Because of this, in the planning stage of the MES, the load carrying capabilities should be considered as a whole to identify the mutual effects among different energy sectors. For an MES planning scheme, its load carrying capability adequacy should be evaluated to guarantee the resilience of the load supply under potential malfunctions.

In power system analysis, the load carrying capability can be effectively depicted by modeling its security region. The security region defines a space where a system can be safely operated under operational and security constraints. For electrical power systems, different types of security regions have been proposed. Wu et al. [4] proposed a practical algorithm for the power system steady-state security region based on fixed-point iteration for the first time. Ou et al. [5] proposed a method to evaluate the available transfer capability and margins of the power system. Chiang et al. [6] investigated the characteristics and applications of the feasible region of optimal power flow. Nguyen et al. [7]

* Corresponding author.
E-mail address: ningzhang@tsinghua.edu.cn (N. Zhang).

https://doi.org/10.1016/j.ijepes.2020.106551
Received 31 May 2020; Received in revised form 11 August 2020; Accepted 21 September 2020
Available online 15 October 2020

Nomenclature

Symbols of Energy Hub

$\boldsymbol{\Phi}_v$	Energy Flow Feasible Set
$\boldsymbol{\Phi}_{v,i}$	Energy Flow Feasible Set under *i*-th Contingency
$\boldsymbol{A}_g$	Port-Branch Incidence Matrix of Node *g*
$\boldsymbol{C}_{in}$	Input Incidence Matrix
$\boldsymbol{C}_{out}$	Output Incidence Matrix
$\boldsymbol{H}_g$	Converter Characteristic Matrix of Node *g*
$\boldsymbol{V}$	Energy Flow Vector
$\boldsymbol{V}_i$	Energy Flow Vector under *i*-th Contingency
$\boldsymbol{V}_{in}$	Energy Input Vector
$\boldsymbol{V}_{out}$	Energy Output Vector
$\boldsymbol{Z}$	Energy Conversion Matrix of Energy Hub
$\boldsymbol{Z}_g$	Energy Conversion Matrix of Node *g*
B	Number of Branches
G	Number of Nodes
K_g	Number of Ports of Node *g*

Symbols of Security Region

$\boldsymbol{\Omega}^*$	Polyhedron Obtained by Proposed Method
$\boldsymbol{\Omega}$	Security Region
$\boldsymbol{\Omega}^{N-1}$	Security Region under N-1 Contingency
$\boldsymbol{\Omega}_i$	Security Region under *i*-th Contingency
$\boldsymbol{F}^*$	Face Set of $\boldsymbol{\Omega}^*$
$\boldsymbol{F}$	Face Set of $\boldsymbol{\Omega}$
$\boldsymbol{P}^*$	Vertex Set of $\boldsymbol{\Omega}^*$
$\boldsymbol{P}$	Vertex Set of $\boldsymbol{\Omega}$
$\mathbf{X}$	State Variable Vector
$\mathbf{X}_i$	State Variable Vector under *i*-th Contingency
$\mathbf{Y}$	Energy Supplying Capacity Vector
$f()$	Operational and Security Constraint Set
$f_i()$	Operational and Security Constraint Set under *i*-th Contingency
N	Number of Components

constructed convex inner approximations of the steady-state security region. Ding et al. [8] proposed a robust bi-level coordinated static voltage security region for centralized wind farms. Zu et al. [9] demonstrated the mathematical base and deduction of the distribution system security region. The security region model has many applications. Chen et al. [10] proposed an assessment method for power system steady-state security based on evaluating the distance to the security region boundaries. Chavez-Lugo et al. [11] proposed a DC optimal power flow model incorporating practical security boundary constraints.

The MES can be divided into two layers, the district MES that covers a small local area such as industrial parks and urban districts and the cross-regional MES that uses electric/gas/thermal transmission systems to connect different district MES [12]. The concept of security regions has also been used in the research on cross-regional MES to deal with the electric-gas and electric-heat coupling. Chen et al. [13] proposed a robust security region for the inter-regional electricity-gas integrated energy system while considering the uncertainty of the wind power. Wei et al. [14] proposed an algorithm to calculate the available transfer capability of the electricity-gas integrated energy systems. Correa-Posada et al. [15] proposed a framework to analyze the energy adequacy of integrated power and gas systems. Pan et al. [16] considered the feasible region in integrated heat and electricity dispatch. Gholizadeh et al. [17] enhanced the demand supply's security using power to gas technology. However, these studies mainly focus on the cross-regional MES and do not consider the energy conversion characteristics.

In this paper, we focus on the district MES where different energy sectors are coupled during its conversion and storage process. Its energy load carrying capability under normal operation and contingency is of great concern during the planning stage. However, due to the mutual effects among different energy sectors, the load carrying capability of each energy form cannot be considered separately. A generalized framework is urgently needed.

To tackle this problem, we propose a systematic way of evaluating the load carrying capability of district MES and demonstrate how it can improve the planning of MES. The district MES is modeled using the Energy Hub (EH) approach [18], which has been successfully applied in the planning, operation and security analysis of district MES [19–23]. In this paper, we propose the concept of the EH steady-state security region to evaluate the load carrying capability of MES. The definition is given first. Then, the corresponding mathematical form is established based on the standardized matrix modeling approach [24]. A vertex-based algorithm is proposed to calculate the security region as a space projection problem. In the planning stage, based on the security region calculation, indices are proposed to evaluate the adequacy of the MES planning schemes under normal operation and contingencies and its critical components can be identified.

This paper makes the following contributions:

1. The steady-state security region of an EH is systematically defined and formulated in a general way to represent the load carrying capability of a district MES.
2. A vertex-based algorithm is proposed to calculate the security region, where the contingencies such as N-1 can be considered.
3. The EH security region analysis is applied to MES planning. Indices based on the security region calculation are proposed to evaluate the planning schemes and identify the critical components.

The remainder of this paper is organized as follows. Section 2 defines the steady-state security region of the EH and formulates the corresponding mathematical form based on EH standardized matrix modeling. The security region model in Section 2 is implicit and cannot be used directly, so Section 3 states a vertex-based algorithm for the security region calculation. Then, the security regions are applied to evaluate the adequacy of MES planning schemes and identify critical components in Section 4. Section 5 shows how the proposed method works on numerical case studies. Finally, conclusions are drawn in Section 6.

2. Definition and modeling

As mentioned above, we model the district MES from the EH perspective. In this section, we first derive the definition of the EH steady-state security region and formulate the generalized mathematical form of the security region (Section 2.1). To systematically depict the energy conversion relationships and build the analytical model between the EH system constraints and the energy supplies, the EH standardized matrix modeling [24] is introduced (Section 2.2). Based on this EH modeling approach, the specified EH steady-state security region is obtained (Section 2.3).

2.1. Definition of the Steady-state security region

For power systems, the definition of the steady-state security region is a set of real and reactive power injections of all nodes, under the condition that the power flow equations and the security constraints of equipment are satisfied [4]. Accordingly, *the steady-state security region of the EH is defined as a set of energy supplying capacities for which the*

operational and security constraints are satisfied.

To evaluate the load carrying capability of the MES, we focus on the output of the EH. Thus, we denote the energy supplying capacities as vector $\mathbf{Y}$, and each component of $\mathbf{Y}$ represents the energy flow at the corresponding output port. $\mathbf{X}$ is the vector of the state variables of the EH. Then, the steady-state security region of the EH can be described as follows:

$$\mathbf{\Omega} = \{\mathbf{Y} | f(\mathbf{X}, \mathbf{Y}) \leqslant \mathbf{0}\} \tag{1}$$

Here, $f(\mathbf{X}, \mathbf{Y}) \leqslant \mathbf{0}$ is the operational&security constraint set of the EH. The operational constraints include the energy conversion equations of the components and the energy flow capacity limits, while the security constraints describe the operation limits of the components in the EH. Note that the equality constraints can also be expressed as inequalities, and the security region $\mathbf{\Omega}$ is modeled in a unified manner. For any $\mathbf{Y} \in \mathbf{\Omega}$, there is at least one $\mathbf{X}$ such that the equality and inequality constraints are satisfied. It is also worth mentioning that $\mathbf{X}$ and $\mathbf{Y}$ do not have a one-to-one correspondence. Furthermore, if the N-1 contingencies are considered, the corresponding constraints should be incorporated, and the security region is narrowed:

$$\mathbf{\Omega}^{N-1} = \{\mathbf{Y} | f_i(\mathbf{X}_i, \mathbf{Y}) \leqslant 0, \ \forall i \in [0, N]\} \tag{2}$$

where i represents the i-th contingency, and $f_i(\mathbf{X}_i, \mathbf{Y}) \leqslant 0$ is the constraint set under the i-th contingency. If $i = 0$, all components are in service.

2.2. Standardized matrix modeling of the EH

In this paper, the standardized matrix modeling [24] is employed to model the steady-state energy conversion relationships of the EH, applying graph theory [25] to cast the topology of the EH and the characteristics of the components. Thus the constraint set $f()$ in Eq. (1) can be specified. This method has the following advantages: it can address the nonlinearity from the dispatch factors by using energy flow as the state variables; based on this model, the EH steady-state security region can be calculated accurately.

The topology of the EH can be expressed by a set of branches, nodes, and ports so that an EH is modeled as an oriented graph, as shown in Fig. 1. Note that the inputs and outputs are treated as special nodes. Each node has multiple ports to exchange energy with other nodes. The energy flows (modeled as branches) are treated as state variables. All energy flows in the EH form an energy flow vector $\boldsymbol{V}$.

Similar to power system analysis, the incidence vectors and matrices are employed to describe the connections.

2.2.1. Port-branch incidence matrices

A port-branch incidence matrix $\boldsymbol{A}_g$ shows the relationship between a node g and all branches in the EH. Assume that there are B branches and G nodes in an EH and the g-th node has K_g ports; then, $\boldsymbol{A}_g$ are defined as follows:

$$\boldsymbol{A}_g(k, b) = \begin{cases} 1 & b \text{ is connected to input port} k \text{ of } g \\ -1 & b \text{ is connected to output port} k \text{ of } g \\ 0 & b \text{ is not connected to any port of } g \end{cases} \tag{3}$$

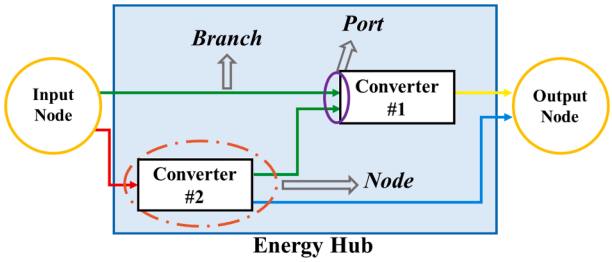

Fig. 1. Illustrative example of the branch, node and port in the EH.

2.2.2. Converter characteristic matrices

The converter characteristic matrix of node g, denoted as $\boldsymbol{H}_g$, represents the energy conversion characteristics of the node. Assume that the node g has K_g ports and the conversion characteristics require P_g equations to describe them; then, the corresponding converter characteristic matrix $\boldsymbol{H}_g$ has a dimension of $P_g \times K_g$.

2.2.3. Energy conversion matrices

The energy conversion matrix is obtained by multiplying the port-branch incidence matrix by the converter characteristic matrix of node g:

$$\boldsymbol{Z}_g = \boldsymbol{H}_g \boldsymbol{A}_g \tag{4}$$

This matrix describes the energy conversion characteristics of node g from the perspective of the branch. The energy conversion matrix of the EH can be obtained by integrating all the node energy conversion matrices:

$$\boldsymbol{Z} = \left[\boldsymbol{Z}_1^T, \ \boldsymbol{Z}_2^T, \ \cdots, \ \boldsymbol{Z}_G^T\right]^T \tag{5}$$

2.2.4. Energy flow equations for the EH

Based on the matrices defined above, the energy conversion equations can be expressed as follows:

$$\boldsymbol{ZV} = \mathbf{0} \tag{6}$$

Here, $\boldsymbol{Z}$ is the EH energy conversion matrix, and $\boldsymbol{V}$ is the energy flow vector, which consists of the branch energy flows. Let $\boldsymbol{V}_{in}$ and $\boldsymbol{V}_{out}$ represent the energy input flows and the energy output flows, respectively. The input incidence matrix $\boldsymbol{C}_{in}$ and output incidence matrix $\boldsymbol{C}_{out}$ are defined as follows:

$$\begin{aligned} \boldsymbol{C}_{in}(i, b) &= \begin{cases} 1 & \text{if input node} i \text{ is the source of branch } b \\ 0 & \text{otherwise} \end{cases} \\ \boldsymbol{C}_{out}(i, b) &= \begin{cases} 1 & \text{if output node} i \text{ is the sink of branch } b \\ 0 & \text{otherwise} \end{cases} \end{aligned} \tag{7}$$

Then, the total energy flow equations of the EH can be expressed in matrix form:

$$\begin{aligned} \boldsymbol{ZV} &= \mathbf{0} \\ \boldsymbol{C}_{in}\boldsymbol{V} &= \boldsymbol{V}_{in} \\ \boldsymbol{C}_{out}\boldsymbol{V} &= \boldsymbol{V}_{out} \end{aligned} \tag{8}$$

Here the first row represents the coupling relationship in the EH, while the second and third rows describe the input and output relationships of the EH, respectively. Additionally, the standardized matrix model can also incorporate the energy storage and integrated demand response. The details can be found in [24].

2.2.5. Energy flow feasible set

The energy flow feasible set $\mathbf{\Phi}_v$ constrains the energy flows by the inequalities that represent the energy transfer limitation of the branches. Moreover, the capacity constraints of the converters in the EH are also embedded in $\mathbf{\Phi}_v$ by setting the respective input or output branch constraints.

2.3. EH steady-state security region modeling

Based on the EH modeling in Section 2.2, the mathematical form of steady-state security region is obtained. According to the definition in Section 2.1, the security region should be a set of energy output vectors $\boldsymbol{V}_{out}$, under the condition that the corresponding constraints are satisfied:

$$\mathbf{\Omega} = \{\boldsymbol{V}_{out} | \boldsymbol{C}_{out}\boldsymbol{V} = \boldsymbol{V}_{out}, \ \boldsymbol{ZV} = \mathbf{0}, \ \boldsymbol{V} \in \mathbf{\Phi}_v\} \tag{9}$$

Furthermore, if the N-1 contingencies are considered in the security region analysis, the energy output vectors $\boldsymbol{V}_{out}$ in the security region $\mathbf{\Omega}$

should satisfy the constraints after an N-1 contingency occurs. Then, the security region considering N−1 contingencies is defined as follows:

$$\boldsymbol{\Omega}^{N-1} = \left\{ \boldsymbol{V}_{out} | \boldsymbol{C}_{out}\boldsymbol{V}_i = \boldsymbol{V}_{out},\ \boldsymbol{Z}\boldsymbol{V}_i = \boldsymbol{0}, \ \boldsymbol{V}_i \in \boldsymbol{\Phi}_{v,i}\ \forall i \in [0, N] \right\} \tag{10}$$

Here, $\boldsymbol{V}_i$ and $\boldsymbol{\Phi}_{v,i}$ are the energy flow vector and its feasible set under the i-th contingency, respectively. In particular, $i = 0$ represents the normal status such that no component is out of service. We denote $\boldsymbol{\Omega}_i$ to be the set such that the corresponding constraints in Eq. (9) are satisfied under the i-th contingency, and then the N-1 security region can be expressed as an intersection of a series of sets:

$$\boldsymbol{\Omega}^{N-1} = \boldsymbol{\Omega}_0 \ \cap\ \boldsymbol{\Omega}_1 \ \cap\ \cdots\ \cap\ \boldsymbol{\Omega}_N \tag{11}$$

2.4. Discussion

2.4.1. Comparison with existing research

Compared with the existing researches [13–16,26], the proposed steady-state security region model has significant differences in threefold: 1) The existing papers focus on the operational and security constraints of energy transmission networks on injections of nodes in the networks, while we focus on the district MES and formulate the security region from the load carrying capability point of view. Such modeling can directly tell whether the system is secure or not under normal or contingency occasions from the load forecast. 2) Some of the research only focuses on the example MES, while this paper provides a general method of formulating the security region that applies to all kinds of district MES. Both the modeling and polyhedron projection method can be highly automated by computers with reliable performance. 3) Beyond the current research, this paper proposes an evaluation methodology that can quantify the load carrying capability of MES. Such evaluation facilitates a direct comparison between different MES planning schemes and can well support the decision making of MES planning.

2.4.2. Extendibility

The EH steady-state security region is modeled using the linear equations. The reasons for using such a linear modeling approach are threefold: 1) We focus on the load carrying capability of the MES in the planning stage, where the linear model is widely used, e.g., power system security regions [9–11]. From the load carrying prospective, the steady-state operational and security constraints of EH can be well linearized. 2) The security region can only be analytically formulated based on the linearized model. Such a method acts as a fundamental basis for the security region analysis under more complex conditions, such as considering the transient processes of the MES. 3) The proposed method can also indirectly handle the nonlinear or non-convex multi-energy system models and this characteristic makes it has good potential to be used in district MES operation studies:

Handling Nonlinear Convex Constraints: In the situation that the operational&security constraint set in Eq. (1) contains nonlinear convex constraints, the security region is still convex. The proposed method is able to calculate an inscribed polyhedron of the security region as close as possible. The details are introduced in Section 3.3.4.

Handling Non-Convex Constraints: The non-convex constraints can be handled in two ways: One is to approximate the original model using convex relaxation, such as the relaxation in the Distflow model [27] for power distribution networks. The other is to segment the non-convex region into several convex sub-regions. Then, our proposed method can be applied to each of the sub-regions. The overall security region is the union of all of the sub-regions.

3. EH security region calculation method

The security region modeled in Section 2 is implicit and cannot be used directly. Thus, getting the explicit form of the security region is necessary for further analysis and applications. The calculation method is proposed in this section.

3.1. Problem statement and property analysis

The security region calculation can be seen as a space projection problem. As defined in Section 2.3, the security region $\boldsymbol{\Omega}$ is a set constrained by constraints in Eq. (9). Define the hyperspace constructed by $\boldsymbol{V}_{out}(K \times 1)$ and $\boldsymbol{V}(B \times 1)$ as the whole hyperspace $\mathbb{R}^K \times \mathbb{R}^B$, and then the constraints in Eq. (9) form a polyhedron $\boldsymbol{G}$ in the hyperspace $\mathbb{R}^K \times \mathbb{R}^B$:

$$\boldsymbol{G} = \left\{ (\boldsymbol{V}_{out}, \boldsymbol{V}) \in \mathbb{R}^K \times \mathbb{R}^B \mid \boldsymbol{C}_{out}\boldsymbol{V} = \boldsymbol{V}_{out}, \ \boldsymbol{Z}\boldsymbol{V} = \boldsymbol{0},\ \boldsymbol{V} \in \boldsymbol{\Phi}_v \right\} \tag{12}$$

The calculation of the security region $\boldsymbol{\Omega}$ is a projection of the polyhedron $\boldsymbol{G}$ in $\mathbb{R}^K \times \mathbb{R}^B$ to its subspace $\mathbb{R}^K$. The Fourier-Motzkin elimination (FME) method [28] is a common algorithm to solve the projection problem. However, the computational complexity of the FME is exponential [29], so it is not capable of complicated power and multi-energy systems. In this paper, a numerical method is developed to calculate the security region. Compared with the FME method, the proposed method does not face the exponential explosion problem and can be used to analyze the multi-energy systems. Note that the security region $\boldsymbol{\Omega}$ has the following properties:

1. $\boldsymbol{\Omega}$ is a polyhedron in $\mathbb{R}^K$: $\boldsymbol{G}$ is a polyhedron in $\mathbb{R}^K \times \mathbb{R}^B$, and $\boldsymbol{\Omega}$ is the projection of $\boldsymbol{G}$ in $\mathbb{R}^K$, so $\boldsymbol{\Omega}$ has this property.
2. For $\forall\ \boldsymbol{V}_{out} \in \boldsymbol{\Omega}, \boldsymbol{V}_{out} \geqslant 0$: Since $\boldsymbol{0} \leqslant \boldsymbol{V}, \boldsymbol{V}_{out} = \boldsymbol{C}_{out}\boldsymbol{V}$.
3. $\boldsymbol{0}$ is one of the vertices of $\boldsymbol{\Omega}$: Let $\boldsymbol{V} = \boldsymbol{0}$ and $\boldsymbol{V}_{out} = \boldsymbol{0}$, and then the constraints in Eq. (9) hold. Thus, $\boldsymbol{0} \in \boldsymbol{\Omega}$. Since $\boldsymbol{V}_{out} \geqslant 0, 0$ cannot be a linear combination of two points in $\boldsymbol{\Omega}$. Moreover, on each axis of $\mathbb{R}^K$, a vertex exists.

A polyhedron in hyperspace can be expressed as an intersection of a set of half-spaces or a convex combination of a set of vertices. The two types of expressions are equivalent, and one expression can be transformed into another [30]:

$$\begin{aligned} &Expression\ 1 : \left\{ \boldsymbol{V}_{out} | \boldsymbol{a}_i^T \boldsymbol{V}_{out} + b_i \leqslant 0,\ \forall \boldsymbol{a}_i, b_i \in \boldsymbol{F} \right\} \Leftrightarrow \\ &Expression\ 2 : \left\{ \boldsymbol{V}_{out} | \boldsymbol{V}_{out} = \sum \lambda_i \boldsymbol{v}_i,\ \lambda_i \geqslant 0, \sum \lambda_i = 1, \boldsymbol{v}_i \in \boldsymbol{P} \right\} \end{aligned} \tag{13}$$

Here, $\boldsymbol{F}$ is the surface set of $\boldsymbol{\Omega}$ and $\boldsymbol{P}$ is the corresponding vertex set.

3.2. Calculation algorithm

A vertex-based algorithm is proposed to calculate the security region $\boldsymbol{\Omega}$. The key point is building an initial polyhedron $\boldsymbol{\Omega}^*$, which is a subset of $\boldsymbol{\Omega}$, and expanding it iteratively to approach $\boldsymbol{\Omega}$. First, a set of vertices lying on the axes of $\mathbb{R}^K$ are obtained, and an initial polyhedron $\boldsymbol{\Omega}^*$ is built. Then, we search new vertices of $\boldsymbol{\Omega}$ along with the normal directions of the surfaces of $\boldsymbol{\Omega}^*$. After a round of searching, $\boldsymbol{\Omega}^*$ is updated using the newly obtained vertices. With the process of searching and updating, $\boldsymbol{\Omega}^*$ grows, approaching $\boldsymbol{\Omega}$. The details of the algorithm are introduced below.

3.2.1. Initializing

We use the vertices on the axes of $\mathbb{R}^K$ and $\boldsymbol{0}$ to initialize the polyhedron $\boldsymbol{\Omega}^*$.

The vertex on the i-th axis of $\mathbb{R}^K$ is calculated with the following linear programming (LP):

$$\begin{aligned} \max \quad & \boldsymbol{e}_i^T \boldsymbol{V}_{out} \\ \text{s.t.} \quad & \boldsymbol{V}_{out} = \boldsymbol{C}_{out} \boldsymbol{V} \\ & \boldsymbol{Z}\boldsymbol{V} = \boldsymbol{0} \\ & \boldsymbol{V} \in \boldsymbol{\Phi}_v \end{aligned} \tag{14}$$

Here, $\boldsymbol{e}_i = [0, 0, \cdots, 1, \cdots, 0]^T$ is the i-th unit basis vector of $\mathbb{R}^K$. This LP finds the largest value along the i-th axis, subjected to the constraints of the EH, and the result of LP is the objective vertex.

After the LPs, $\boldsymbol{\Omega}$'s vertices, which are on the axis, are obtained. We use these vertices, along with $\boldsymbol{0}$, to construct a vertex set $\boldsymbol{P}^*$. The corresponding polyhedron $\boldsymbol{\Omega}^*$ can be built as Eq. (15). Since $\boldsymbol{P}^* \subset \boldsymbol{P}$, the polyhedron $\boldsymbol{\Omega}^*$ is a subset of $\boldsymbol{\Omega}$.

$$\boldsymbol{\Omega}^* = \left\{ \boldsymbol{V}_{out} | \boldsymbol{V}_{out} = \sum \lambda_i \boldsymbol{v}_i,\ \lambda_i \geqslant 0, \sum \lambda_i = 1, \boldsymbol{v}_i \in \boldsymbol{P}^* \right\} \tag{15}$$

3.2.2. Expanding

Denote the surface set of $\boldsymbol{\Omega}^*$ as $\boldsymbol{F}^*$, and based on $\boldsymbol{F}^*$, new vertices of $\boldsymbol{\Omega}$ are searched and discovered.

For every surface in $\boldsymbol{F}^*$, we search the vertex along with its normal direction. Assume that $\boldsymbol{d}_j$ is the unit normal direction vector of the j-th surface in $\boldsymbol{F}^*$, the following LP is calculated:

$$\begin{aligned} \max \quad & \boldsymbol{d}_j^T \boldsymbol{V}_{out} \\ \text{s.t.} \quad & \boldsymbol{V}_{out} = \boldsymbol{C}_{out} \boldsymbol{V} \\ & \boldsymbol{Z}\boldsymbol{V} = \boldsymbol{0} \\ & \boldsymbol{V} \in \boldsymbol{\Phi}_v \end{aligned} \tag{16}$$

If the optimal solution $\boldsymbol{V}_{out}^*$ is not in $\boldsymbol{P}^*$, a new vertex of $\boldsymbol{\Omega}$ has been discovered. If the LP has more than one optimal vertex, which means Eq. (16) has infinite optimal solutions, we choose only one vertex as the optimal solution. In contrast, if the optimal solution $\boldsymbol{V}_{out}$ is in the vertex set $\boldsymbol{P}^*$, the search would not provide a new vertex.

3.2.3. Updating

After an expanding round, newly discovered vertices are added to $\boldsymbol{P}^*$. Then, $\boldsymbol{\Omega}$ is improved. According to Eq. (13), the surface set $\boldsymbol{F}^*$ is updated correspondingly. After updating, a new expanding round starts. The iteration will stop if a new vertex is not found in an expanding round, and thus $\boldsymbol{\Omega}^* = \boldsymbol{\Omega}$.

The flowchart for the security region calculation is formulated in Fig. 2.

Fig. 3 shows an example of the proposed algorithm. Assume that an EH provides electricity and heat jointly and that the output space is two-dimensional. The security region $\boldsymbol{\Omega}$ of this EH is shown in Fig. 3.1. To calculate $\boldsymbol{\Omega}$, we first search the vertices along the axes (as in Fig. 3.2) and initialize $\boldsymbol{\Omega}^*$ (as in Fig. 3.3). From the surface of $\boldsymbol{\Omega}^*$, a new vertex is searched along the normal direction (as in Fig. 3.4). Then, $\boldsymbol{\Omega}^*$ is updated using the newly found vertex (as in Fig. 3.5), and a new round of vertex searching starts. On different surfaces of $\boldsymbol{\Omega}^*$, we search the vertex of $\boldsymbol{\Omega}$ along the corresponding normal directions (as in Fig. 3.6 and Fig. 3.7). Then, $\boldsymbol{\Omega}^*$ is updated (as in Fig. 3.8). Since $\boldsymbol{\Omega}^* = \boldsymbol{\Omega}$, there is no vertex of $\boldsymbol{\Omega}$ that does not belong to $\boldsymbol{\Omega}^*$. In the next expanding round, no vertex would be found, and the algorithm stops.

As expressed in Eq. (11), if N-1 contingencies are considered, the intersection needs to be calculated. Assume $\boldsymbol{\Omega}_i$ to be the security region calculated under the j-th contingency:

$$\boldsymbol{\Omega}_j = \left\{ \boldsymbol{V}_{out} | \boldsymbol{a}_{(j)i}^T \boldsymbol{V}_{out} + b_{(j)i} \leqslant 0,\ \forall \boldsymbol{a}_{(j)i}, b_{(j)i} \in \boldsymbol{F}_j \right\} \tag{17}$$

Then, the output vector $\boldsymbol{V}_{out}$ should satisfy the constraints in all $\boldsymbol{\Omega}_j$. The intersection of these regions can be obtained in the following way:

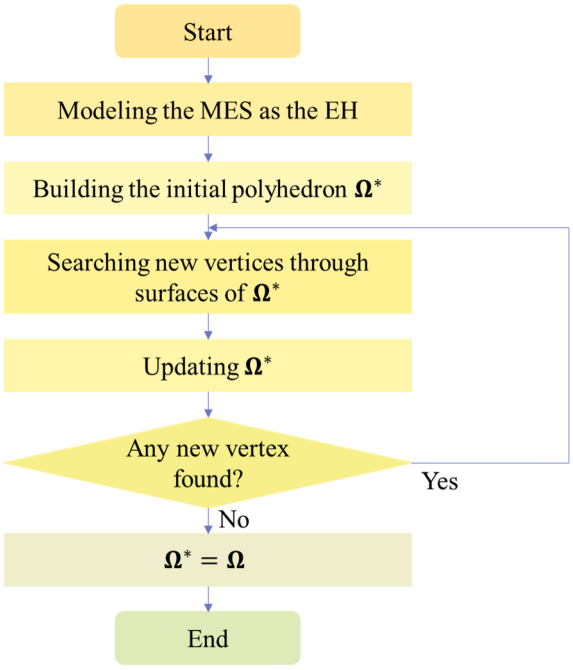

Fig. 2. The flowchart of the proposed algorithm.

$$\begin{aligned} \boldsymbol{\Omega}^{N-1} = & \quad \boldsymbol{\Omega}_0 \cap \boldsymbol{\Omega}_1 \cap \cdots \cap \boldsymbol{\Omega}_N \\ = & \quad \left\{ \boldsymbol{V}_{out} | \boldsymbol{a}_{(j)i}^T \boldsymbol{V}_{out} + b_{(j)i} \leqslant 0, \right. \\ & \left. \forall \boldsymbol{a}_{(j)i}, b_{(j)i} \in \boldsymbol{F}_{\mathbf{j}},\ j = 0, 1, \cdots, N \right\} \end{aligned} \tag{18}$$

3.3. Discussion

There are several properties of the proposed algorithm that guarantee that the algorithm is effective in solving the projection problem and building the security region $\boldsymbol{\Omega}$ precisely.

3.3.1. Validity

It is guaranteed that all vertices obtained by the proposed method are extreme points of the security region $\boldsymbol{\Omega}$. Otherwise, the optimal solution of Eq. (16) $\boldsymbol{V}_{out}^*$ can be expressed as a linear combination of the extreme points:

$$\boldsymbol{V}_{out}^* = \sum \lambda_i \boldsymbol{v}_i,\ 0 \leqslant \lambda_i < 1, \sum \lambda_i = 1, \boldsymbol{v}_i \in \boldsymbol{P} \tag{19}$$

If there is only one extreme point $\boldsymbol{v}^*$ such that $\boldsymbol{d}^T \boldsymbol{v}^* = \max \boldsymbol{d}^T \boldsymbol{v}_i,\ \boldsymbol{v}_i \in \boldsymbol{P}$, then $\boldsymbol{d}^T \boldsymbol{v}^* > \sum \lambda_i \boldsymbol{v}_i = \boldsymbol{d}^T \boldsymbol{V}_{out}^*$, and $\boldsymbol{V}_{out}^*$ is not the optimal solution, which contradicts the assumption.

If there are two extreme points $\boldsymbol{v}^{*(1)}$ and $\boldsymbol{v}^{*(2)}$ such that $\boldsymbol{d}^T \boldsymbol{v}^{*(1)} = \boldsymbol{d}^T \boldsymbol{v}^{*(2)} = \max \boldsymbol{d}^T \boldsymbol{v}_i,\ \boldsymbol{v}_i \in \boldsymbol{P}$, then the optimization problem Eq. (16) has infinite solutions. In this case, an extreme point of Eq. (16) is chosen as the optimal solution, and it is also an extreme point of $\boldsymbol{\Omega}$.

3.3.2. Convergence

The security region in the hyperspace $\mathbb{R}^K$ is a polyhedron and has finite vertices. If the algorithm is terminated after a round of searching, a new vertex is not discovered in this round. Then, all vertices of $\boldsymbol{\Omega}$ are in $\boldsymbol{P}^*$, and the obtained polyhedron $\boldsymbol{\Omega}^*$ is equal to $\boldsymbol{\Omega}$. Otherwise, at least one vertex $\boldsymbol{v}$ of $\boldsymbol{\Omega}$ is not discovered after the searching process. In the hyperspace $\mathbb{R}^K$, $\boldsymbol{v}$ belongs to a convex cone defined by K vertices in $\boldsymbol{P}^*$. We denote the normal direction of the corresponding surface defined by the same K vertices as $\boldsymbol{d}$. Because of the convexity of $\boldsymbol{\Omega}$, $\boldsymbol{d}^T \boldsymbol{v}$ is greater than the inner products of $\boldsymbol{d}$ and K vertices, and the searching process in Eq. (16) should find a new vertex. This fact contradicts the assertion of a

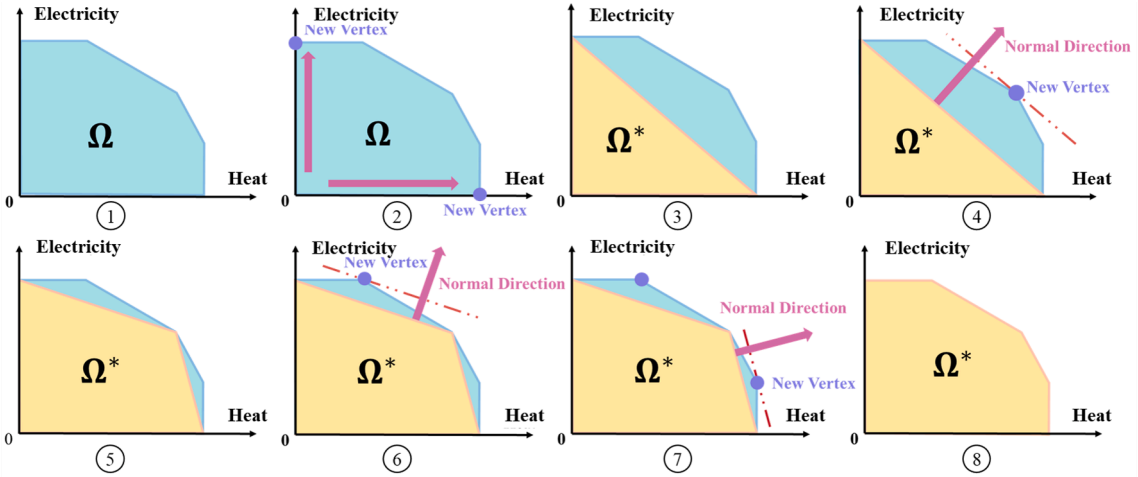

Fig. 3. A demonstration of the proposed algorithm in a 2-dimensional example.

new vertex not being discovered.

As a result, in the searching process, new vertices are discovered, and the number of vertices in $\boldsymbol{P}^*$ is not reduced. Then, the search would terminate in a finite number of iterations on the condition that all vertices are updated to $\boldsymbol{P}^*$.

3.3.3. Parallel computing potential

In the process of expanding the security region, the algorithm needs to search the vertices of $\boldsymbol{\Omega}$ along the normal directions of the surfaces in $\boldsymbol{F}^*$. Thus, the corresponding LPs should be solved. These LPs are independent of each other and it is not necessary to calculate them in sequence. To improve efficiency, a parallel computing architecture can be applied to run the LPs synchronously.

3.3.4. Generality

The proposed method can also be directly applied to MES with convex nonlinear operation constraints. In this case, the security region cannot be described by a polyhedron. However, we can still use the proposed method to find an inscribed polyhedron $\boldsymbol{\Omega}^*$ of the real security region $\boldsymbol{\Omega}$. As iteration increases $\boldsymbol{\Omega}^*$ gradually approaches $\boldsymbol{\Omega}$.

4. Security region applications in planning

The EH steady-state security region can be applied in the planning stage of the district MES. For an MES planning scheme, it is necessary to evaluate its accuracy. This can be achieved by calculating its corresponding security region. Then, 4 indices based on the security region calculation result are proposed in this section to analyze the load carrying capability of a planning scheme and identify its corresponding critical components. According to these indices, the accuracy of an MES planning scheme can be evaluated from a security region perspective and the planning scheme can be improved guided by the critical component identification.

4.1. Volume of the Security Region (VSR)

The EH steady-state security region represents the outputs in the output space $\mathbb{R}^K$, where the corresponding constraints are satisfied. In the hyperspace, we define the hypervolume of the polyhedron $\boldsymbol{\Omega}$ as the volume of the corresponding security region:

$$VSR_{\Omega} = \int_{\Omega} dv = \int \cdots \int_{\Omega} dx_1 dx_2 \cdots dx_k \tag{20}$$

The multiplicity of the integral depends on the dimension of the hyperspace $\mathbb{R}^K$. In practice, this multiple integral can be calculated by Monte Carlo methods.

The volume of the security region measures the size of the load demand space that the EH can deliver. It reflects the multiple energy load carrying capability from a macroscopic perspective. The absolute value of the VSR does not have a direct physical meaning, but can be used to make comparisons among different planning schemes of the same MES.

4.2. Load-Weighted Volume (LWV)

In MES planning, the load demand of different kinds of energy should be considered. Each point in the output space $\mathbb{R}^K$ represents a load demand scenario of the MES, but its corresponding occurrence probability varies. The load-weighted volume (LWV) evaluates the ratio of scenarios in which all kinds of load demands can be served. Compared with the VSR, the LWV takes the distribution of the load demand into consideration. Assume that the joint probability density of different kinds of load demands is p_d. Then, the load-weighted volume can be expressed as follows:

$$LWV_{\Omega} = \int_{\Omega} p_d \, dv \times 100\% = \int \cdots \int_{\Omega} p_d \, dx_1 dx_2 \cdots dx_k \tag{21}$$

A higher LWV indicates a greater probability of serving all kinds of loads. From another perspective, the LWV can also be explained as a "biased volume integral" of the security region weighted by the load distribution.

In Eq. (20) and Eq. (21), if the security region $\boldsymbol{\Omega}$ is replaced by $\boldsymbol{\Omega}^{N-1}$, the corresponding VSR and LWV can be calculated with the consideration of the N-1 contingency.

4.3. Critical component identification

The components in an EH hold different positions, and their contributions to the load carrying capability vary. Some components have a great influence on the security region, and an outage could shrink the volume of the region significantly, while some components are less important since their function can be replaced by auxiliary or redundant components.

In this paper, we define two indices to identify the critical components. The important degree of volume (IDV) measures a component's influence on the VSR, and the important degree of load (IDL) measures its influence on the LWV:

$$\begin{aligned} IDV_i &= (1 - \frac{VSR_i}{VSR_0}) \times 100\% \\ IDL_i &= (1 - \frac{LWV_i}{LWV_0}) \times 100\% \end{aligned} \tag{22}$$

where VSR_0 and LWV_0 are the volumes of the security region and load satisfaction rate when all components are in service, while VSR_i and LWV_i are the corresponding indices if the i-th component is out of service, respectively. The components with higher IDVs or IDLs are more important to the security region and the load carrying capability.

The IDVs and IDLs could guide the MES planning by identifying the most critical component. The load carrying capability of an MES can be effectively improved by enhancing the critical component. The possible measurements include the following: 1) improving the reliability of the critical component; 2) replacing the critical component with multiple smaller units of the same total capacity to diversify the risks; and 3) increasing the capacity of the critical component to ensure the redundancy.

5. Case studies

Numerical case studies are conducted on test systems to illustrate the effectiveness of the proposed algorithm. Then their corresponding load carrying capabilities and critical components are analyzed. All of the analyses are implemented using MATLAB with CPLEX and Multi Parametric Toolbox (MPT) [31].

5.1. Test System 1

In this subsection, an illustrative example is presented, in which the details of the proposed method are discussed. The test system is an EH that consists of a combined heat and power unit (CHP), an auxiliary boiler (AB), and an electricity transformer, providing two kinds of energy, heat, and electricity to consumers. The topology of the EH is shown in Fig. 4 and the capacities and efficiencies of the components are listed in Table 1.

The outputs of Test System 1 are heat and electricity, so the security region is in a two-dimensional space. Applying the standardized matrix modeling method introduced in Section 2.2, the energy conversion matrix, the input incidence matrix, and the output incidence matrix are constructed correspondingly. The security region is calculated using the proposed method in Section 3.2 and the FME method [28]. The security regions obtained by these two methods are equivalent, which proves the validity of the proposed method. The results are shown in Fig. 5. The x-axis represents the heat output of the EH, while the y-axis represents the electricity output.

Fig. 5.1 presents an example of the security region if all components are available. The security region is a pentagon in two-dimensional space. Every point in the pentagon represents an EH output state in which all constraints are satisfied, and the boundary of the pentagon shows the maximum load carrying capability of Test System 1. In Fig. 5.2, the blue rectangle shows the security region of Test System 1 when the CHP is unavailable. Taking the outage of the CHP into consideration, the load carrying capability of Test System 1 decreases, and the security region shrinks from the original pentagon to the blue rectangle. Fig. 5.3 and Fig. 5.4 show the security region if the AB and the transformer are unavailable, respectively. To consider the N-1 contingency, the intersection of the polyhedrons above are calculated according to Eq. (18), and the security region $\mathbf{\Omega}^{N-1}$ is shown in Fig. 5.5.

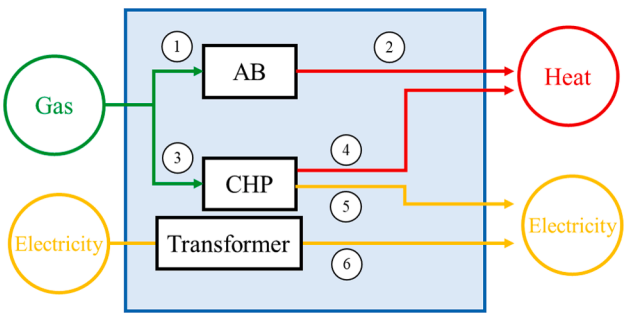

Fig. 4. The topology of the EH in Test System 1.

Table 1
Installed capacities and energy efficiencies of the components in Test System 1.

Component	Capacity (MW)	Efficiency
CHP	20	El: 0.3 Therm: 0.4
AB	10	0.9
Transformer	10	–

The VSR of $\mathbf{\Omega}$ is 248 MW^2, while the VSR of $\mathbf{\Omega}^{N-1}$ is 48 MW^2. When the N-1 contingency is considered, the VSR shrinks by 80.6%, from 248 to 48 MW^2. This is because Test System 1 has only 3 energy converters and the topology is less than complicated. Thus, the system lacks redundancy, and when an N-1 contingency occurs, the position of the outage component cannot be substituted by other components.

The proposed method can also be extended to non-linear and non-convex situations. If the CHP works in extraction condensing operation mode and the operation constraints are non-linear and non-convex (as in Fig. 6), the method described in Section 2.4 can be applied: 1) Segment the non-convex region into two convex sub-regions (Area 1 and Area 2 in Fig. 6). 2) Apply the proposed method on the convex sub-regions respectively. 3) Calculate the union of all of the sub-regions. The results are shown in Fig. 7. In particular, Fig. 7.1 shows the region calculated using Area 1; Fig. 7.2 shows the region calculated using Area 2; Fig. 7.3 is the aggregation of them, which is the entire security region while the CHP works in extraction condensing operation mode.

5.2. Test System 2

Test system 2 is an EH that contains multiple kinds of energy converters and storage equipment, including two CHPs, two water absorption refrigerator groups (WARG), two compression electric refrigerator groups (CERG), an electric heat pump (EHP), an AB, a power to gas (P2G), a cooling storage (CS), a heat storage (HS), a gas storage (GS), and two power transformers. The topology is shown in Fig. 8 and the capacities and efficiencies of the components are listed in Table 2. The load data of this system is a one-year period of multiple load demands for a park in Beijing, China.

The corresponding matrices are constructed applying the standardized matrix modeling. Then, the proposed method is employed to calculate the security region and corresponding indices. To calculate the $\mathbf{\Omega}$, 6 rounds of iterations are carried out, and in each round, we found 1, 3, 5, 8, 4 and 3 new vertexes respectively. The searching process is shown in Fig. 9. By using the proposed method, the calculation of $\mathbf{\Omega}$ only takes 0.18 s. However, it is beyond the capacity of FME method [28] because of the exponential computational complexity.

Fig. 10 shows the security region of Test System 2, where the three axes represent the outputs of the electricity, cooling, and heat, respectively. The security regions with and without consideration of the N-1 contingency are both calculated. For Test System 2, the output space is three-dimensional, and the security region is a 3D convex polyhedron. The VSR of $\mathbf{\Omega}$ is 1.70×10^7 MW^3, while the VSR of $\mathbf{\Omega}^{N-1}$ is 5.73×10^6 MW^3. When the N-1 contingency is considered, the VSR is shrunk by 66.3%.

From the load demand curve, the LWV of the security region can be calculated, which evaluates the load carrying capability for the real load demand. For $\mathbf{\Omega}$, the LWV is 100%, which means that the load demand can be served by Test System 2 at all times, on the condition that all components are in service. Without considering component outages, Test System 2 is a planning scheme whose load carrying capability is large enough to satisfy the given load. However, the LWV of $\mathbf{\Omega}^{N-1}$ is 98.59%, so 1.41% of the load demand is in $\mathbf{\Omega}$ but out of $\mathbf{\Omega}^{N-1}$. This proportion of the load demand is exposed to a load shedding risk when

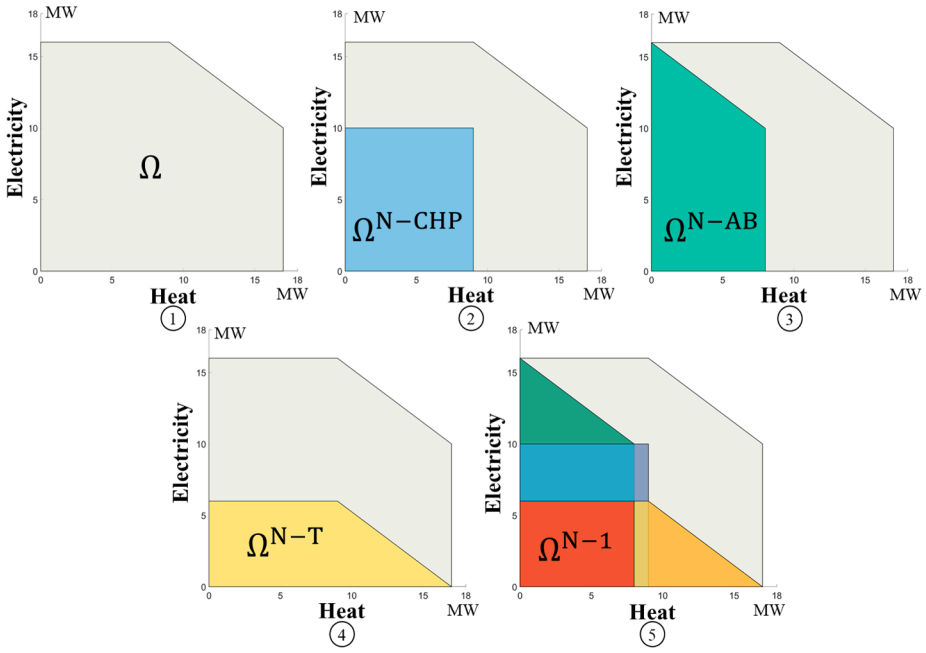

Fig. 5. The security region of Test System 1.

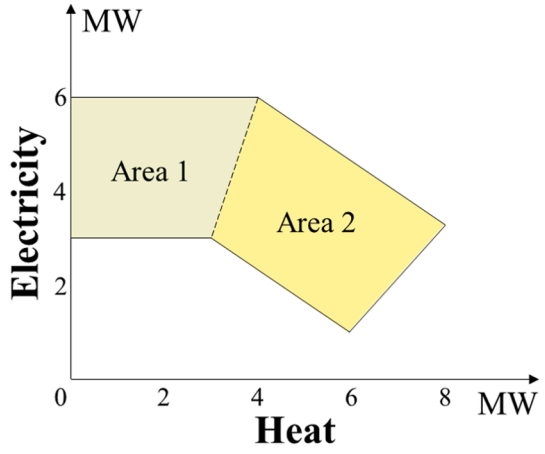

Fig. 6. The operation constraints of the extraction condensing mode CHP.

an N-1 contingency occurs.

Comparing the VSR and the LWV, they both evaluate the load carrying capability of an MES planning scheme, but the latter index takes the load demand distribution into consideration. The VSR depicts the "volume" of the security region, while the LWV presents the proportion of situations that all load can be served. They describe the load carrying capability from different perspectives.

The critical component identification methods are applied to Test System 2. The IDL and IDV indices of the components calculated according to Section 4.3 are listed in Fig. 11. The results show that CHP1 and CHP2 are the most critical components, and there is a slight difference in IDV_{CHP1} and IDV_{CHP2} because of the topology of Test System 2. T1 and T2 are the second most important components. These components have the same IDV and IDL because they are planned to operate in parallel and have identical topology. The CERGs, WARGs, AB, and CS also make respective contributions. To improve the planning scheme,

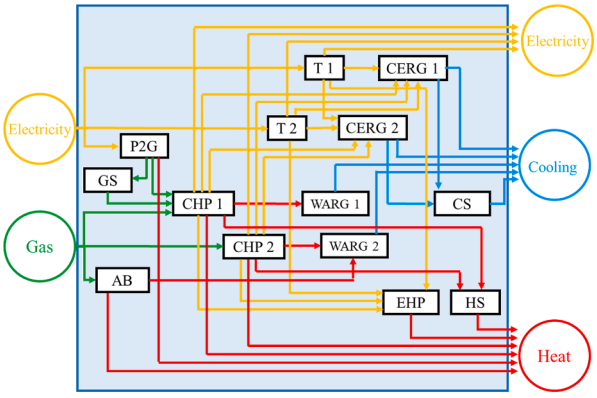

Fig. 8. The topology of the EH in Test System 2.

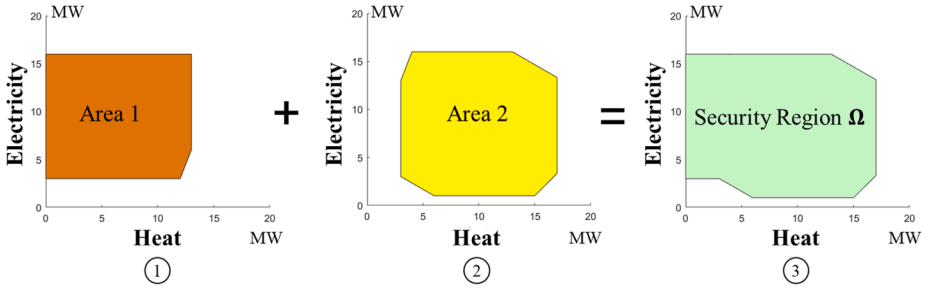

Fig. 7. The security region when CHP in extraction condensing operation mode.

Table 2
Installed capacities and energy efficiencies of the components in Test System 2.

Component	Capacity (MW)	Efficiency
CHP	240	El: 0.3 Therm: 0.45
WARG	70	0.7
CERG	24	3
EHP	16	3
AB	50	0.8
P2G	50	Gas: 0.58 Therm: 0.12
CS	60	0.9
HS	30	0.9
GS	30	1
Transformer	70	–

the reliability of the CHPs and transformers could be improved so that their outage possibilities are reduced. Another method is to replace a critical component with more components of the same type. For example, the planning scheme can be adjusted by removing CHP1 and adding two CHPs with a capacity of 120 MW. Then, the total installation capacity remains the same, but they can both be in mutual standby. After the adjustment, the VSR of $\boldsymbol{\Omega}$ is still 1.70×10^7 MW^3, but the VSR of $\boldsymbol{\Omega}^{N-1}$ increases to 7.48×10^6 MW^3, which is improved by 30.5%.

6. Conclusions and future work

This paper provides insights on load carrying capability of a district MES by the concept of the EH steady-state security region. It is able to systematically formulate the load carrying capability considering the coupling of different forms of energy. The district MES is modeled using EH standardized matrix modeling. An effective vertex-based algorithm is proposed to calculate the security region as a polyhedron in a hyperspace. The results demonstrate that the proposed method is able to evaluate the adequacy of district MES planning schemes and find critical components that affect the load carrying capability. The security of MES can be greatly improved by enhancing the critical components. Further study includes taking into account the nonlinearity of the EH and embedding security region constraints in the planning model.

CRediT authorship contribution statement

Pei Yong: Methodology, Software, Validation, Investigation, Data curation, Writing - original draft, Visualization. **Yi Wang:** Writing - review & editing. **Tomislav Capuder:** Writing - review & editing. **Zhenfei Tan:** Writing - review & editing. **Ning Zhang:** Conceptualization, Writing - review & editing, Supervision. **Chongqing Kang:** Writing - review & editing, Supervision.

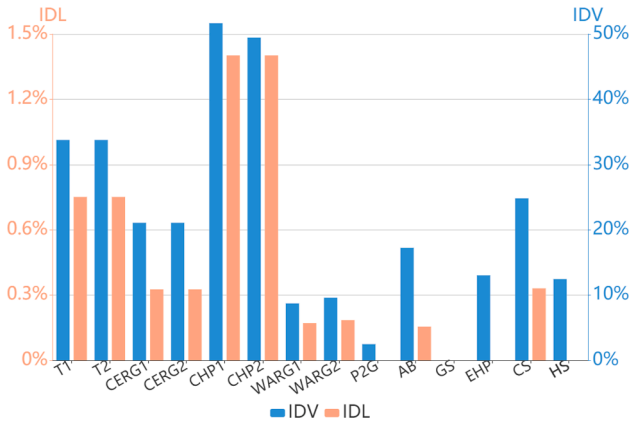

Fig. 11. Indices of the critical component identification in Test System 2.

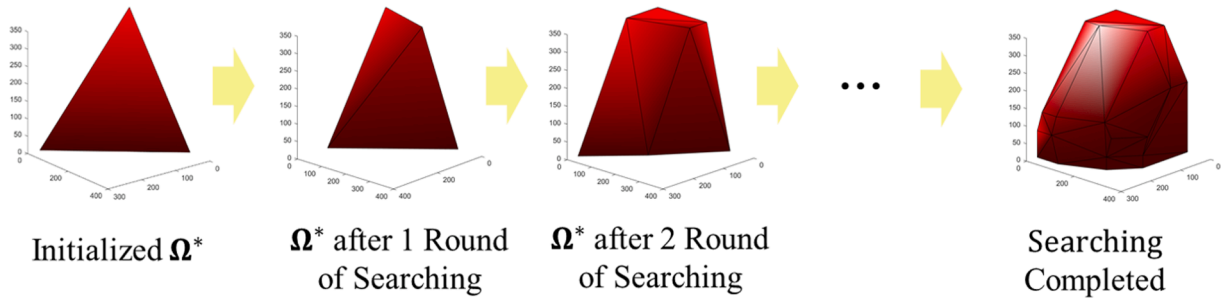

Fig. 9. The searching process of Test System 2.

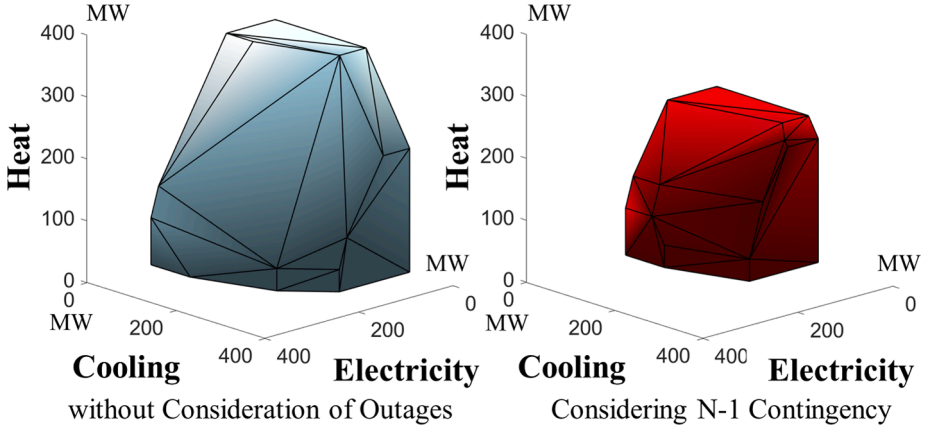

Fig. 10. The security region of Test System 2.

Declaration of Competing Interest

The authors declare that they have no known competing financial interests or personal relationships that could have appeared to influence the work reported in this paper.

Acknowledgement

This work was supported in part by the National Natural Science Foundation of China and State Grid (No. 52061635101), Tsinghua University Initiative Scientific Research Program (20193080026), and the Ministry of Science and Technology International Cooperation Project: Eighth China-Croatia Cooperation Committee Project "Flexible integrated demand response in multi-energy system - FIRE".

References

[1] Krause T, Andersson G, Frohlich K, Vaccaro A. Multiple-energy carriers: modeling of production, delivery, and consumption. Proc IEEE 2011;99(1):15–27.
[2] Mancarella P. MES (multi-energy systems): an overview of concepts and evaluation models. Energy 2014;65:1–17.
[3] Heitkoetter W, Medjroubi W, Vogt T, Agert C. Regionalised heat demand and power-to-heat capacities in germany – an open dataset for assessing renewable energy integration. Appl Energy 2020;259:114161.
[4] Wu F, Kumagai S. Steady-state security regions of power systems. IEEE Trans Circuits Syst 1982;29(11):703–11.
[5] Ou Y, Singh C. Assessment of available transfer capability and margins. IEEE Trans Power Syst 2002;17(2):463–8.
[6] Chiang H, Jiang C. Feasible region of optimal power flow: characterization and applications. IEEE Trans Power Syst 2018;33(1):236–44.
[7] Nguyen HD, Dvijotham K, Turitsyn K. Constructing convex inner approximations of steady-state security regions. IEEE Trans Power Syst 2019;34(1):257–67.
[8] Ding T, Bo R, Sun H, Li F, Guo Q. A robust two-level coordinated static voltage security region for centrally integrated wind farms. IEEE Trans Smart Grid 2016;7(1):460–70.
[9] Zu G, Xiao J, Sun K. Mathematical base and deduction of security region for distribution systems with DER. IEEE Trans Smart Grid 2018:1.
[10] Chen SJ, Chen QX, Xia Q, Kang CQ. Steady-state security assessment method based on distance to security region boundaries. IET Gen Transm Distrib 2013;7(3):288–97.
[11] Chávez-Lugo M, Fuerte-Esquivel CR, Cañizares CA, Gutierrez-Martinez VJ. Practical security boundary-constrained DC optimal power flow for electricity markets. IEEE Trans Power Syst 2016;31(5):3358–68.
[12] Geidl M. Integrated modeling and optimization of multi-carrier energy systems, Ph. D. thesis, eidgenössische technische hochschule zürich; 2007.
[13] Chen S, Wei Z, Sun G, Wei W, Wang D. Convex hull based robust security region for electricity-gas integrated energy systems. IEEE Trans Power Syst 2018:1.
[14] Wei Z, Chen S, Sun G, Wang D, Sun Y, Zang H. Probabilistic available transfer capability calculation considering static security constraints and uncertainties of electricity-gas integrated energy systems. Appl Energy 2016;167:305–16.
[15] Correa-Posada CM, Sánchez-Martín P. Integrated power and natural gas model for energy adequacy in short-term operation. IEEE Trans Power Syst 2015;30(6):3347–55.
[16] Pan Z, Guo Q, Sun H. Feasible region method based integrated heat and electricity dispatch considering building thermal inertia. Appl Energy 2017;192:395–407.
[17] Gholizadeh N, Vahid-Pakdel M, Mohammadi-ivatloo B. Enhancement of demand supply's security using power to gas technology in networked energy hubs. Int J Electric Power Energy Syst 2019;109:83–94.
[18] Geidl M, Koeppel G, Favre-Perrod P, Klockl B, Andersson G, Frohlich K. Energy hubs for the future. IEEE Power Energ Mag 2007;5(1):24–30.
[19] Martínez Ceseña EA, Mancarella P. Energy systems integration in smart districts: Robust optimisation of multi-energy flows in integrated electricity, heat and gas networks. IEEE Trans Smart Grid 2019;10(1):1122–31.
[20] Huo D, Blond SL, Gu C, Wei W, Yu D. Optimal operation of interconnected energy hubs by using decomposed hybrid particle swarm and interior-point approach. Int J Electric Power Energy Syst 2018;95:36–46.
[21] Parisio A, Vecchio CD, Vaccaro A. A robust optimization approach to energy hub management. Int J Electric Power Energy Syst 2012;42(1):98–104.
[22] Zhang X, Shahidehpour M, Alabdulwahab A, Abusorrah A. Optimal expansion planning of energy hub with multiple energy infrastructures. IEEE Trans Smart Grid 2015;6(5):2302–11.
[23] Pazouki S, Haghifam M-R. Optimal planning and scheduling of energy hub in presence of wind, storage and demand response under uncertainty. Int J Electric Power Energy Syst 2016;80:219–39.
[24] Wang Y, Zhang N, Kang C, Kirschen DS, Yang J, Xia Q. Standardized matrix modeling of multiple energy systems. IEEE Trans Smart Grid 2019;10(1):257–70.
[25] Diestel R. Graph theory. Math Gazette 2000;173(502):67–128.
[26] Liu L, Wang D, Hou K, jie Jia H, yuan Li S. Region model and application of regional integrated energy system security analysis. Appl Energy 2020;260:114268.
[27] Baran ME, Wu FF. Network reconfiguration in distribution systems for loss reduction and load balancing. IEEE Trans Power Del 1989;4(2):1401–7.
[28] Bertsimas D, Tsitsiklis J. Introduction to linear optimization, Belmont, MA. USA: Athena Scientific; 1997.
[29] Jahromi AA, Bouffard F. On the loadability sets of power systems part I: Characterization. IEEE Trans Power Syst 2017;32(1):137–45.
[30] Tan Z, Zhong H, Wang J, Xia Q, Kang C. Enforcing intra-regional constraints in tie-line scheduling: a projection-based framework. IEEE Trans Power Syst 2019;34(6):4751–61.
[31] Kvasnica M, Grieder P, Baotić M. Multi-Parametric Toolbox (MPT); 2004. http://control.ee.ethz.ch/mpt/.